Supplementary information for:

A sustainable strategy for fabricating porous carbon supported Sn submicron spheres by self-generated Na_2CO_3 as templates for lithium-ion batteries anode

Kun Liu[a,1], Jia-ao Wang[b,1], Hongfei Zheng[c], Shuhan Guo[a], Xiaofei Wang[a], Jianzong Man[a], Xinyu Wang[a], Juncai Sun[a,*]

[a]Institute of Materials and Technology, Dalian Maritime University, Dalian 116026, China

[b]Department of Chemistry and the Oden Institute for Computational Engineering and Sciences, The University of Texas at Austin, Austin, TX, 78712-0165, USA

[c]Department of Materials, Xiamen University, Xiamen 361005, China

[1] These authors contributed equally to this work.

***Corresponding author:** sunjc@dlmu.edu.cn (J. Sun)

Supplementary Figures

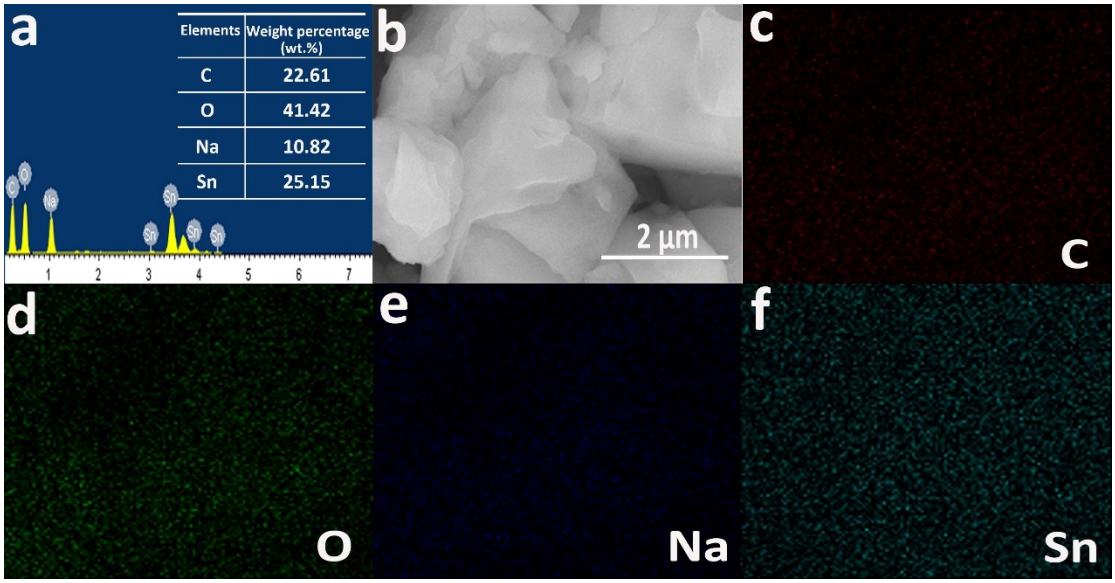

Fig. S1. The basic information of DSSC.

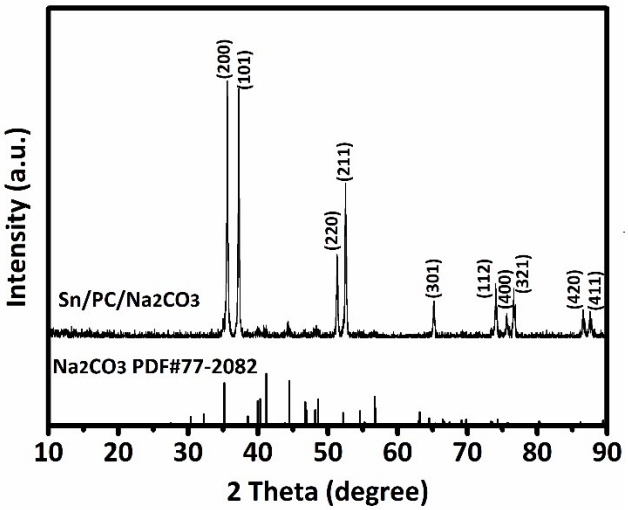

Fig. S2. XRD pattern of unwashed Sn/PC/Na_2CO_3 after carbonization.

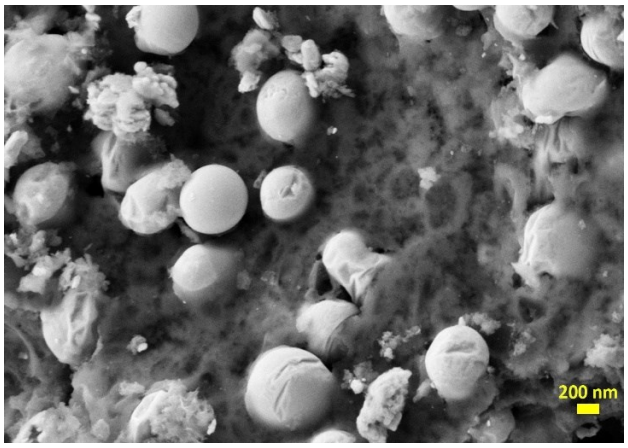

Fig. S3. FE-SEM image of Sn/PC after carbonized at 650 °C.

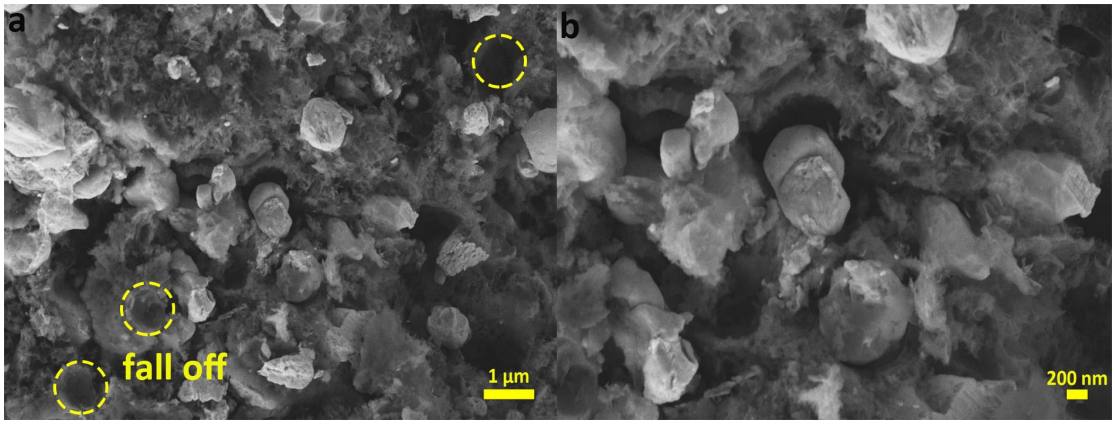

Fig. S4. FE-SEM image of Sn/PC after carbonized at 850 °C.

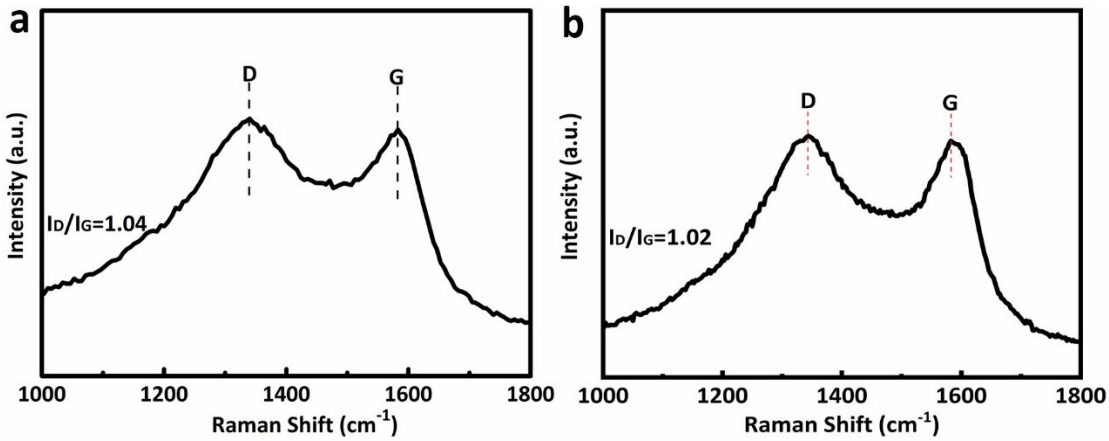

Fig. S5. Raman spectra of (a) Sn/PC and (b) Sn/PC-850.

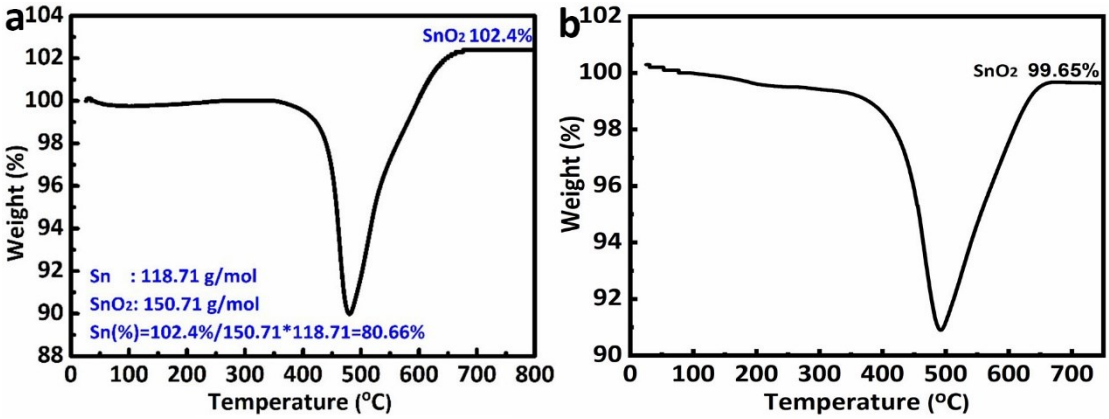

Fig. S6. TGA curves of (a) Sn/PC and (b) Sn/PC-850.

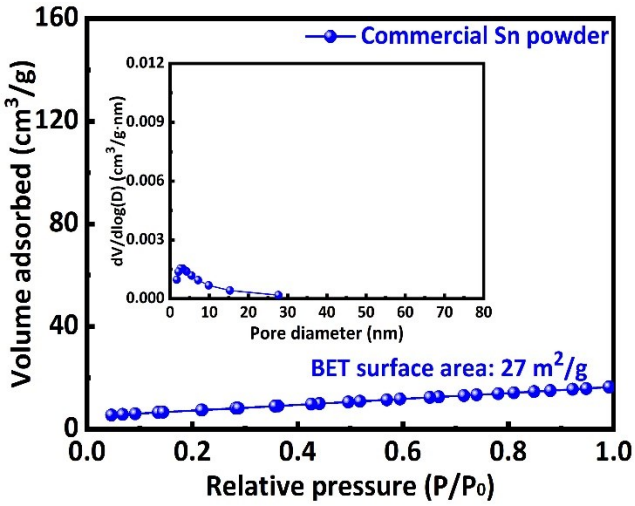

Fig. S7. N_2 adsorption/desorption isotherm of commercial Sn powder (the inset shows pore size distribution curves).

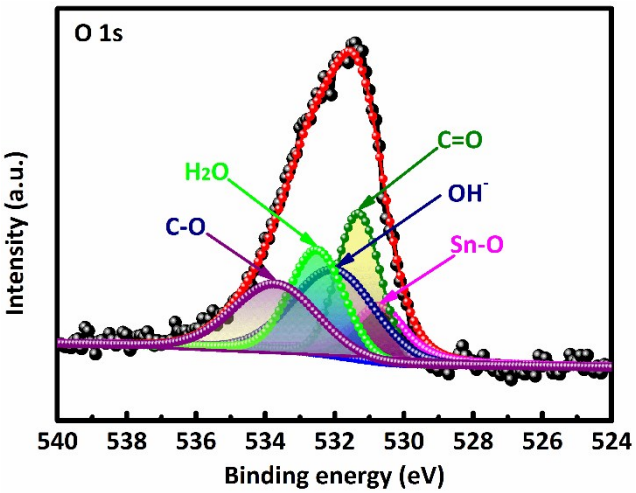

Fig. S8. O 1s spectra of XPS.

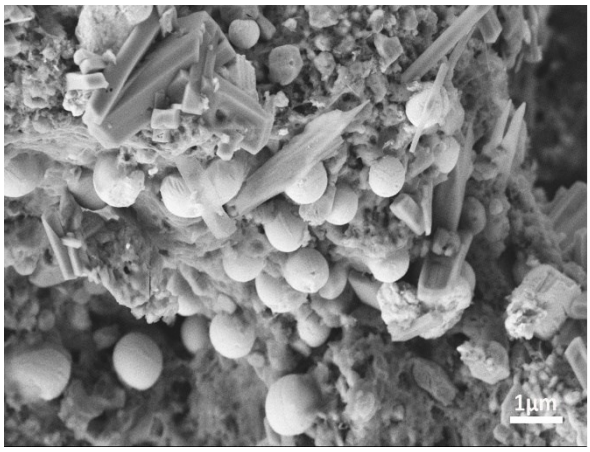

Fig. S9. FE-SEM image of unwashed Sn/PC/Na_2CO_3 after carbonization.

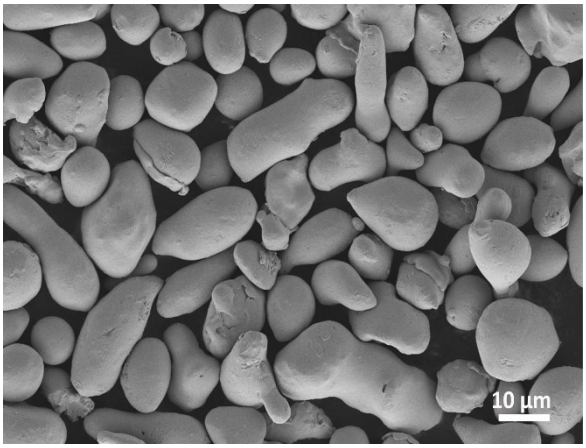

Fig. S10. FE-SEM image of commercial Sn powder.

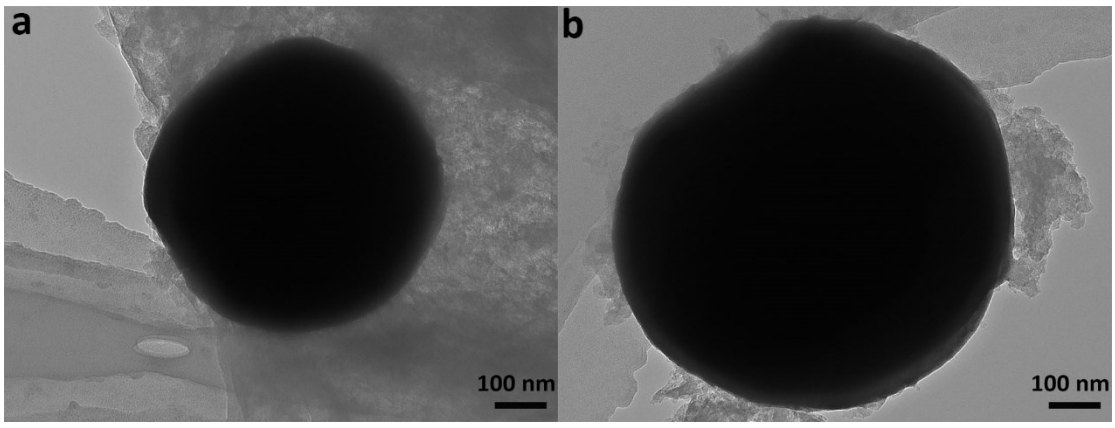

Fig. S11. TEM images of (a) Sn/PC and (b) Sn/PC-850.

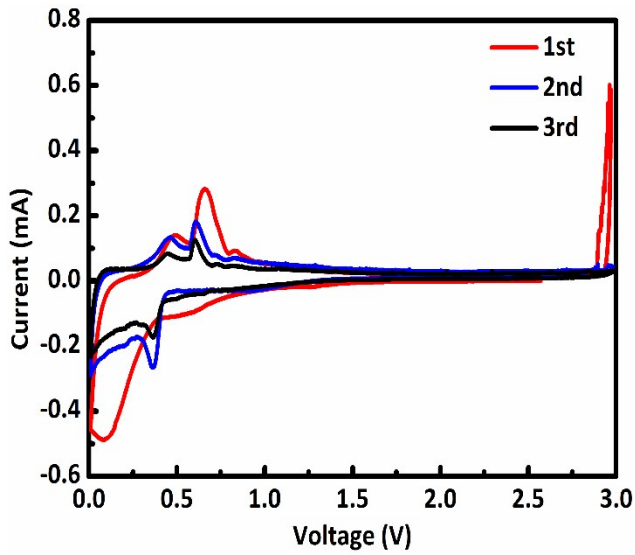

Fig. S12. CV curves of commercial Sn powder.

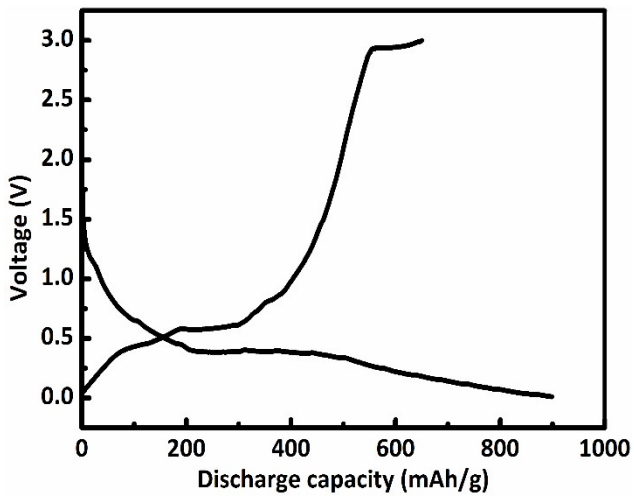

Fig. S13. Initial discharge/charge curve of commercial Sn powder at 100 mA/g.

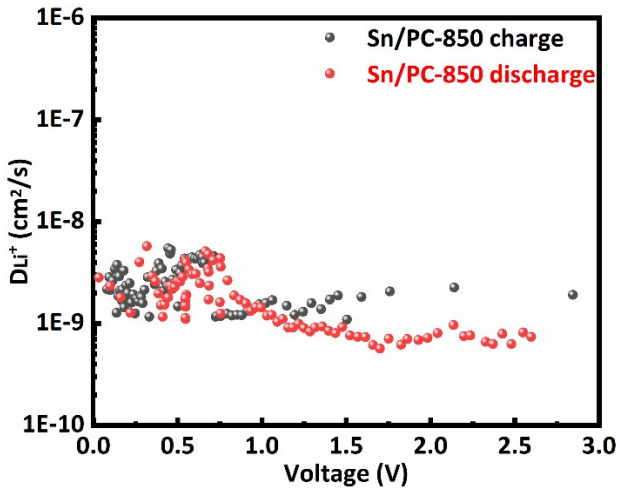

Fig. S14. The Li^+ diffusion coefficient of Sn/PC-850.

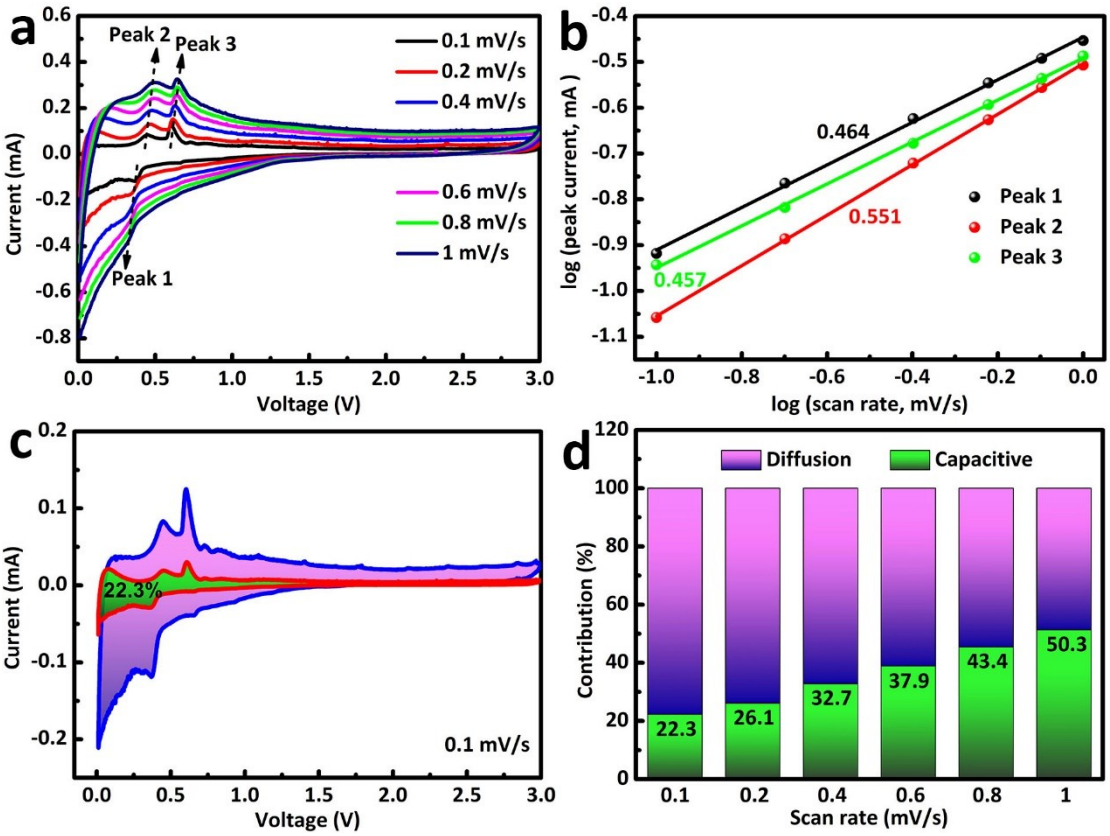

Fig. S15. (a) CV curves of commercial Sn powder at various scan rates from 0.1 to 1 mV/s. (b) The corresponding log(*i*) versus log(*v*) plots at each redox peak. (c) CV curve at 0.1 mV/s with the capacitive contribution to the total current. (d) The ratio of capacitive and diffusion-controlled contribution at various sweep rates.

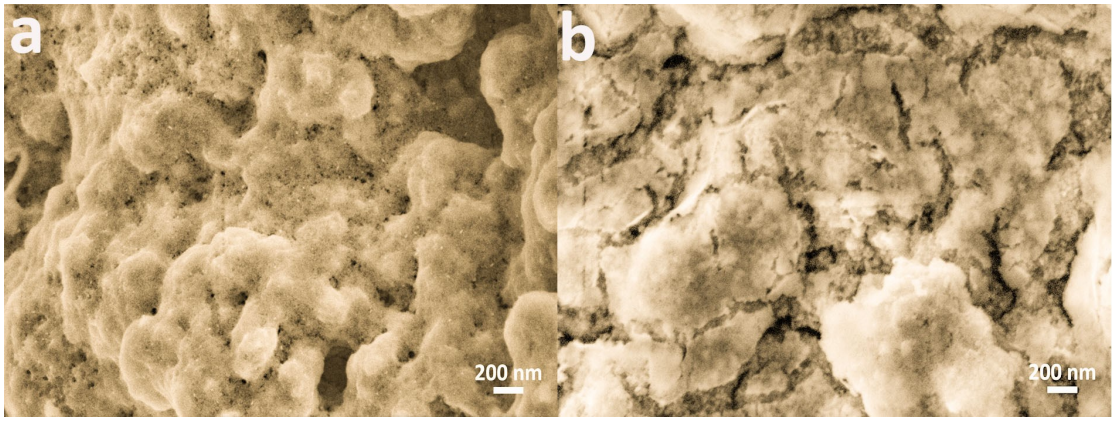

Fig. S16. Morphological characterization after cycling: The SEM images of (a) Sn/PC and (b) commercial Sn powder after 200 cycles at 100 mA/g.

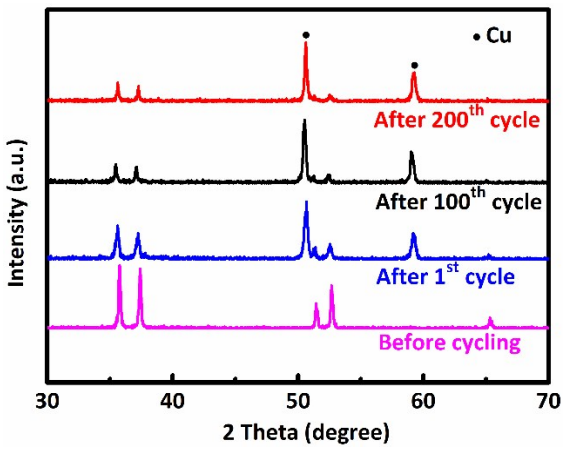

Fig. S17. XRD patterns of Sn/PC after cycling.

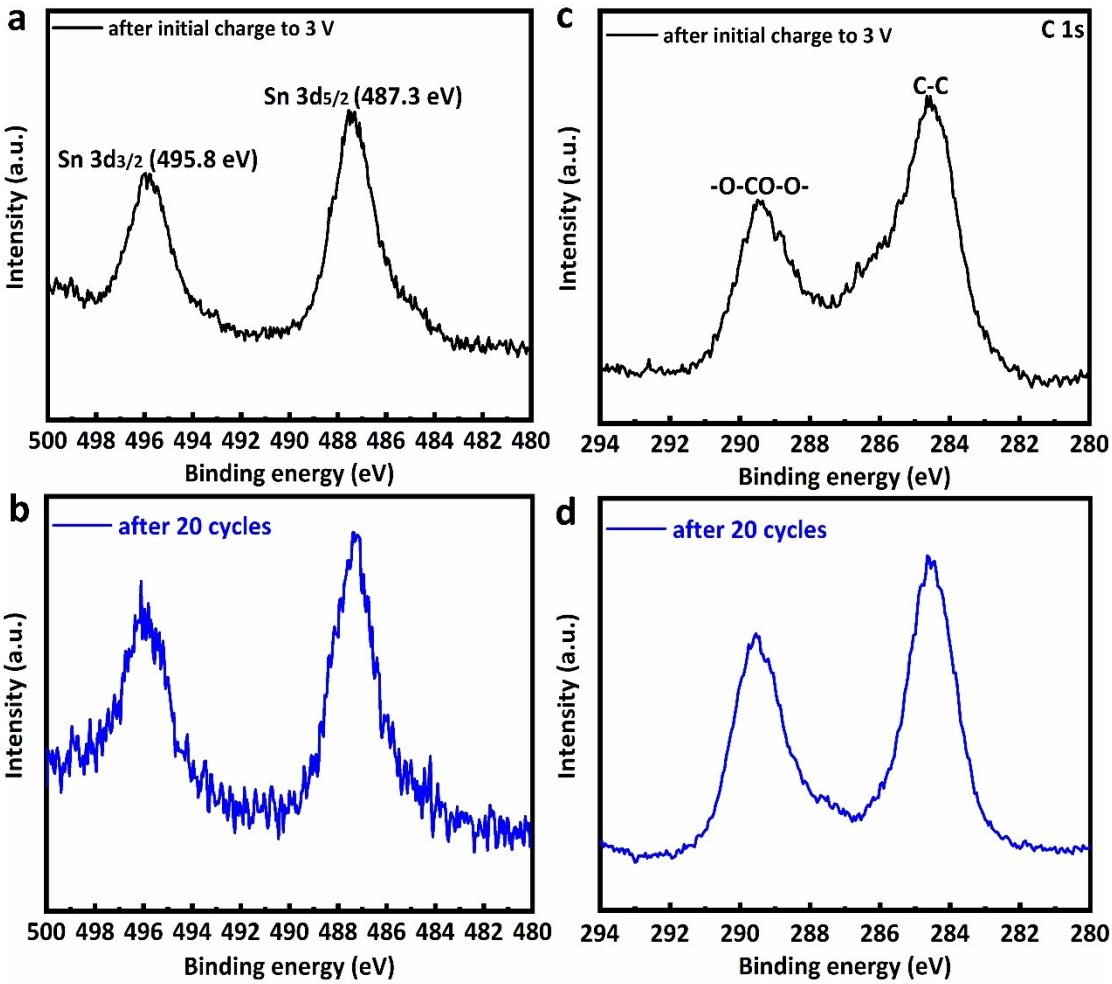

Fig. 18. Ex-situ XPS spectra of Sn/PC electrode after initial charge to 3 V and after 20 cycles: (a-b) Sn 3d; (c-d) C 1s.

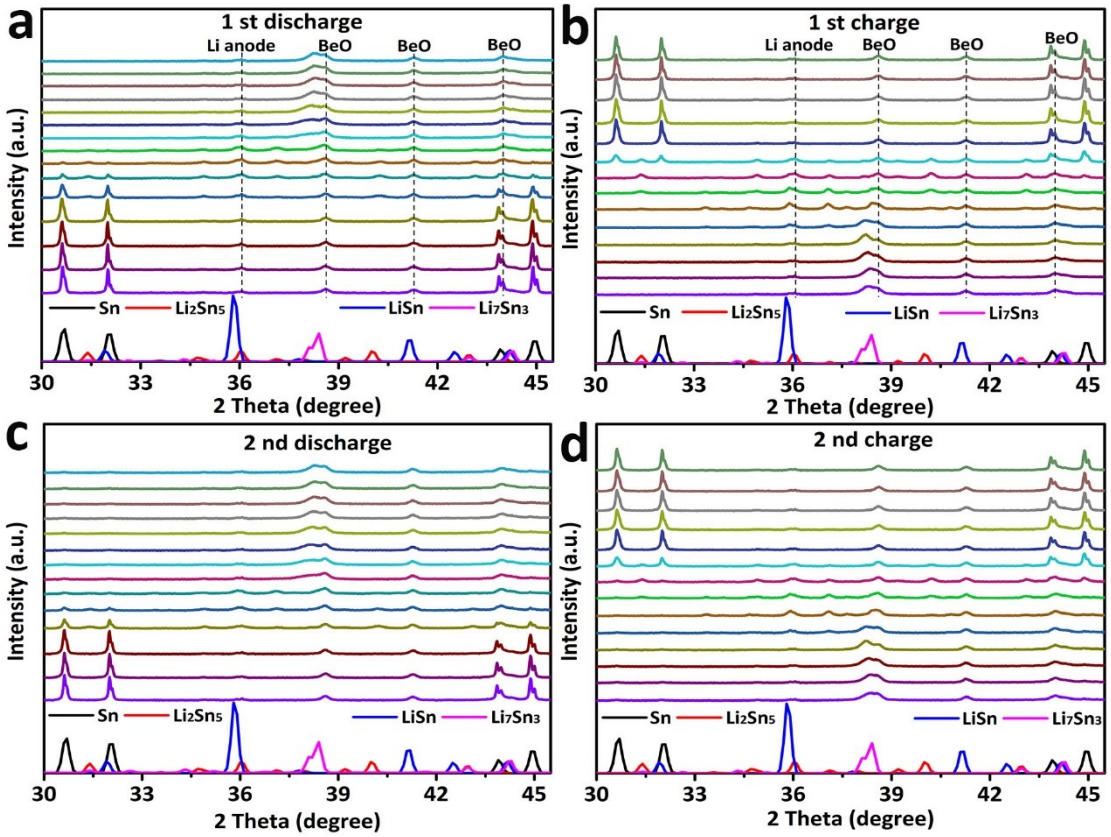

Fig. S19. In-situ XRD patterns of Sn/PC electrode recorded during initial two galvanostatic charge-discharge cycles (100 mA/g).

Table S1. Comparison of the obtained results in this work with previously reported electrochemical performance of Sn-based composite electrodes for LIBs.

Materials	Current (mA/g)	Cycle Number	Capacity (mAh/g)	The wastes and hazardous reagents	Ref.
Sn/C core/shell	40	100	546.7	DMF, Tin (II) 2-ethylhexanoate, Anhydrous ethanol, Acetic acid	[1]
C/Sn	100	500	501	Ethanol, Furfural	[2]
Sn/Graphene	100	100	~500	Hydrazine hydrate, Concentrated H_2SO_4, Concentrated H_3PO_4, H_2O_2, $KMnO_4$	[3]
Sn/G/GNS	100	200	557	Concentrated H_2SO_4, Concentrated H_3PO4, H_2O_2, $KMnO_4$, HCl, $NaBH_4$	[4]
Sn@C	50	100	520	Absolute ethanol, Formaldehyde, Dimethylformamide (DMF)	[5]
Sn–Ni–Cu	100	50	533	Choline chloride, Ethylene glycol, 1 M HCl	[6]
Sn–Ni@C/G	100	100	503	KCl byproduct, Ethanol	[7]
Sn@2DLMG	100	200	539	Tri(propylene glycol) diacrylate, 1-Hydroxycyclohexyl phenyl ketone	[8]
Sn@Ti3C2Tx	100	200	586.38	Hydrochloric acid, Sodium borohydride	[9]
Porous C/Sn	20	15	~420	NaOH, DMF, Formaldehyde	[10]
Sn-CNF	100	50	~400	DMF, Ethanol	[11]
Sn/PC	**100**	**200**	**588**	**Na_2CO_3 template, No hazardous reagents**	**This work**

References

[1] Z. Yang, Q. Meng, W. Yan, J. Lv, Z. Guo, X. Yu, Z. Chen, T. Guo, R. Zeng, *Energy,* 2015, ***82*,** 960–967.

[2] Y. Cheng, Z. Yi, C. Wang, Y. Wu, L. Wang, *Chem. Eng. J.,* 2017, **330,** 1035–1043.

[3] F.R. Beck, R. Epur, D. Hong, A. Manivannan, P.N. Kumta, *Electrochim. Acta,* 2014, **127,** 299–306.

[4] J. Zhu, X. Ding, *J. Alloy. Compd.,* 2019, **809,** 151870–151877.

[5] X. Tao, R. Wu, Y. Xia, H. Huang, W. Chai, T. Feng, Y. Gan, W. Zhang, *ACS Appl. Mater. Interfaces,* 2014, **6,** 3696−3702.

[6] S.C. Rao, X.L. Zou, S.J. Wang, T.Y. Shi, Y. Lu, L. Ji, H.Y. Hsu, Q. Xu, X.G. Lu, *J. Electrochem. Soc*., 2019, **166,** D427–D434.

[7] H. Zhang, M.R. Zhang, M.L. Zhang, L. Zhang, A.P. Zhang, Y.M. Zhou, P. Wu, Y.W. Tang, *J. Colloid Interface Sci.,* 2017, **501,** 267–272.

[8] S. Ding, W. Cheng, L. Zhang, G. Du, X. Hao, G. Nie, B. Xu, M. Zhang, Q. Su, C.A. Serra, *J. Colloid Interface Sci.,* 2021, **589**, 308–317.

[9] Q. Yang, Y. Xia, G. Wu, M. Li, S. Wan, P. Rao, Z. Wang, *J. Alloy. Compd*. 2021, **859**, 157799–157806.

[10] Y. Xu, Y. Zhu, Y. Liu, C. Wang, *Adv. Energy Mater.* 2013, **3**, 128.

[11] H. Wang, J. Zhou, J. Sun, Y. Wang, Y. Ma, Z. Bai, Y. Zhao, W. Zhang, *Int. J. Electrochem. Sci.,* 2020, **15**, 9849–9863.